

GPU-to-Grid: Voltage Regulation via GPU Utilization Control

Zhirui Liang, Jae-Won Chung, Mosharaf Chowdhury, Jiasi Chen, Vladimir Dvorkin

Abstract—While the rapid expansion of data centers poses challenges for power grids, it also offers new opportunities as potentially flexible loads. Existing power system research often abstracts data centers as aggregate resources, while computer system research primarily focuses on optimizing GPU energy efficiency and largely ignores the grid impacts of optimized GPU power consumption. To bridge this gap, we develop a GPU-to-Grid framework that couples device-level GPU control with power system objectives. We study distribution-level voltage regulation enabled by flexibility in LLM inference, using batch size as a control knob that trades off the voltage impacts of GPU power consumption against inference latency and token throughput. We first formulate this problem as an optimization problem and then realize it as an online feedback optimization controller that leverages measurements from both the power grid and GPU systems. Our key insight is that reducing GPU power consumption alleviates violations of lower voltage limits, while increasing GPU power mitigates violations near upper voltage limits in distribution systems; this runs counter to the common belief that minimizing GPU power consumption is always beneficial to power grids.

Index Terms—Distribution voltage regulation, data centers, GPU flexibility, batch size, online feedback optimization.

I. INTRODUCTION

The rapid expansion of AI workloads is driving a sharp rise in data center electricity demand and GPU power density. Globally, data centers consumed about 415 TWh in 2024 and are projected to more than double by 2030, with AI as a key growth driver [1]. At the device level, state-of-the-art accelerators already approach server-scale power intensities (e.g., NVIDIA’s H100 SXM5 GPU specifies up to 700 W per GPU [2]), so large GPU clusters can add multi-megawatt loads over short deployment timelines. This surge creates significant challenges for power-system operation and planning: load growth is geographically concentrated, often constrained by latency and reliability requirements, and can substantially change regional demand trajectories [3].

At the same time, grid-connected data centers also offer new opportunities for power system operation. Similar to vehicle-to-grid (V2G) technologies [4], large-scale data centers can act as flexible demand-side resources by adjusting power consumption in response to grid conditions. Recent work in the power system literature has explored the use of data center flexibility for services such as peak shaving, frequency regulation, and voltage support [5]–[7]. However, most existing studies model data center flexibility at an aggregate level and do not explicitly capture how such flexibility is realized at the device level. In particular, the mechanisms by which GPU workloads provide controllable power adjustments, along with the associated inference latency and throughput constraints, are often abstracted or neglected. These GPU-level considerations

are critical in practice, as they enable fine-grained and fast power control while limiting the achievable magnitude and speed of power adjustments.

From the computer systems perspective, significant effort has been devoted to improving the energy efficiency of GPUs through workload-aware control. Both training and inference energy consumption can be reduced by tuning available control knobs, such as GPU frequency scaling, power caps, and batch size selection, which directly affect utilization, throughput, and latency [8]–[10]. While these methods optimize energy or performance under fixed workload objectives, they do not account for grid needs. From the power system standpoint, there are operating conditions under which increased GPU power consumption is desirable, for example during periods of high renewable generation or when overvoltage arises in distribution networks. Enabling GPUs to act as grid-supportive resources therefore requires closing the loop between grid conditions and device-level control decisions.

To bridge this gap, we propose a GPU-to-Grid (G2G) framework that couples device-level GPU control with grid-level feedback. The framework integrates detailed models of GPU power–performance trade-offs with real-time grid signals, enabling GPUs to operate as grid-supportive resources while respecting computing constraints. Such grid feedback signals may take the form of voltage measurements, frequency deviations, or price signals, depending on the grid service being provided.

In this paper, we focus on a single grid service, i.e., distribution-level voltage regulation, and a single GPU control knob, i.e., the batch size of LLM inference tasks, to demonstrate the G2G framework. The overall G2G system architecture is shown in Fig. 1. Users submit inference requests for heterogeneous LLM models at stochastic arrival rates, which are processed by dedicated GPUs in the data center. This processing results in an inference latency for users, while the resulting GPU power consumption influences the nodal voltage of the connected distribution network. At each control interval, the batch size controller must therefore be both grid- and user-aware, respecting voltage constraints from the power system and latency constraints from inference service users, while the data center operator simultaneously seeks to maximize throughput. The resulting batch size decision reflects a trade-off among grid reliability, user quality-of-service, and data center performance, and is jointly optimized within the proposed G2G framework at each time step.

Several studies have investigated grid services using device-level models of data center resources. For instance, Chen et al. [11] employ GPUs for voltage regulation via dynamic voltage and frequency scaling (DVFS), but assumes a linear relationship between GPU frequency and power and adopts a simple droop-based control that ignores inference latency

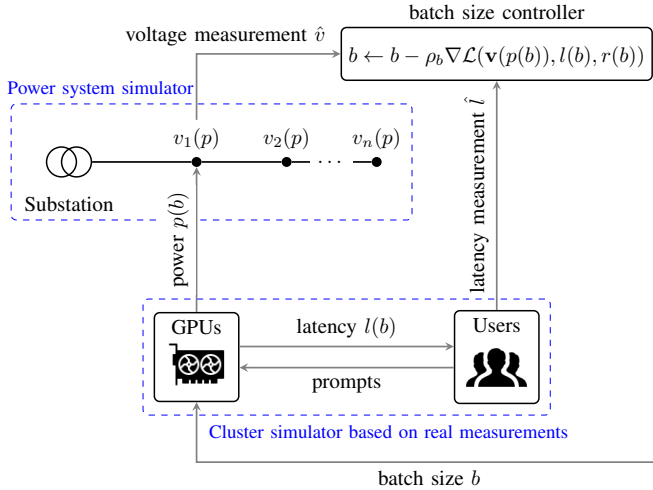


Fig. 1. GPU-to-Grid (G2G) framework for voltage regulation. The aggregated GPU behavior is simulated based on real measurement data in [13], and grid feedback is provided by the power system simulator (e.g., OpenDSS [14]).

and throughput constraints. In contrast, Colangelo et al. [12] demonstrate grid-interactive AI data centers in a field deployment, showing that workload control and DVFS can reduce power consumption during peak periods while maintaining quality of service; however, the grid feedback in that work is limited to high-level exogenous signals such as congestion or peak-demand indicators, rather than physical states of power systems. This work addresses these limitations by using real GPU measurement data to model the nonlinear relationships between control knobs and performance metrics, and by proposing an online-feedback-optimization framework that explicitly incorporates voltage, latency, and throughput. By closing the loop with physical grid measurements and avoiding reliance on demand-response signals, the proposed approach enables fast distribution voltage regulation.

II. ANALYSIS OF GPU MEASUREMENT DATA

A. Data Source and Inference Workload Characterization

Our work is based on real measurements from software, hardware, and workloads that are representative of modern AI data center operations. Specifically, we used the ML.ENERGY Benchmark v3.0 data [10], [13], which provides detailed GPU power consumption, latency, and throughput measurements over time for various batch size¹ configurations of the large language model (LLM) inference server.

Measurements were collected on vLLM [15] v0.11.1 on NVIDIA H100 80GB SXM5 GPUs connected with NVSwitch, both of which are representative of modern AI data centers. Workloads include dense Transformer [16]-based LLMs (Meta Llama 3.1 family [17]) responding to ChatGPT-style conversational queries and mixture-of-experts (MoE) [18] LLMs (Qwen 3 family [19]) answering challenging problems with reasoning, as summarized in Table I. The models used span a variety of architectures, tasks, sizes, number of GPUs, and

¹We refer to the LLM inference server's maximum batch size configuration as simply batch size. With sustained request arrival, the server's real batch size is at or near this maximum batch size.

parameter precisions, providing substantial diversity in power consumption and performance characteristics.

TABLE I
LLMs STUDIED IN THIS PAPER

Model name	Type	Active params [†]	Precision	#GPUs
Llama 3.1 8B	Dense	8B	BF16	1
Llama 3.1 70B	Dense	70B	BF16	4
Llama 3.1 405B	Dense	405B	FP8	8
Qwen3 30B A3B	MoE	3B	BF16	2
Qwen3 235B A22B	MoE	22B	BF16	8

[†]MoE models dynamically activate only a subset of total parameters.

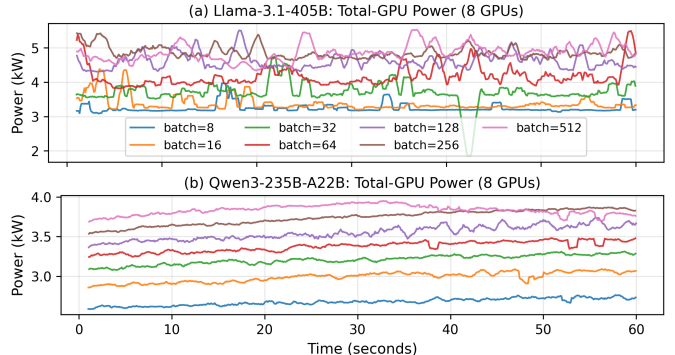


Fig. 2. Aggregated power trajectories across batch sizes for the Llama 3.1 405B and Qwen3 235B A22B models.

Fig. 2 compares the GPU power consumption trajectories over time across different batch sizes for the Llama 3.1 405B and Qwen3 235B A22B models. Both models exhibit a consistent trend: larger batch sizes result in higher average GPU power consumption. This shared property is the foundation of batch size-based control across model architectures.

B. Tradeoff between Latency and Throughput

Inference serving performance is commonly characterized by two key metrics: (1) latency, which quantifies the response time of individual inference requests, and (2) throughput, which measures the total number of requests completed per unit time. When it comes to LLMs, Inter-Token Latency (ITL) is a common latency metric, defined as the time spent to generate each output token after the previous one; a long ITL manifests as an AI chat service speaking very slowly, degrading user experience [20]. For throughput, token throughput is commonly reported, defined as the number of tokens generated per unit time; a low token throughput means that the server is not able to serve as many users at the same time, making users wait longer to get responses.

In LLM serving, tokens are generated in *batches* [21]; b requests run inference together in the GPU, and when the *whole* batch has completed execution by the GPU, each request gets one new token generated (thus b new tokens are generated simultaneously). When the *batch size* b is increased, the raw amount of computation needed to execute inference for that batch increases. This naturally takes more time for the GPU to complete, thereby increasing ITL. On the other hand, with a larger batch size, the GPU's various software

and hardware overheads are better amortized and the GPU's utilization increases, making it capable of completing *more* computations per unit time, increasing token throughput. A side effect of increased GPU utilization is increased power draw, as shown in Fig. 2. The relationship between ITL, token throughput, and batch size for a single LLM text generation iteration can be captured by the following equation:

$$\text{Token Throughput (tokens/s)} = \frac{\text{Batch Size (tokens)}}{\text{Inter-Token Latency (s)}}$$

Ideally, data center operators would want both high throughput and low latency. However, these objectives are inherently in tension because increasing batch size improves throughput while simultaneously increasing latency. We analyze and model this tradeoff relationship and the impact of batch size using real measurement data in Section II-C, and build our optimization model based on this relationship in Section III.

C. Relationship between Performance Metrics and Batch Size

Establishing a closed-form relationship between the control variable (batch size) and GPU performance metrics is essential for the control framework proposed in this paper. To this end, we use GPU measurement data to identify these relationships empirically. Let b denote the batch size of an LLM inference task. Based on the observed measurements, we model the dependence of batch size on (i) total GPU power consumption p (in watts), (ii) mean inter-token latency l (in seconds), and (iii) token throughput r (in tokens per second) using logistic functions. This functional form captures the transition of GPU inference workloads from an underutilized regime to a resource-saturated regime as batch size increases.

Define the logarithmic batch size variable $x \triangleq \log_2(b)$. Then the power consumption, latency, and throughput are modeled directly as functions of x :

$$p(x) = \frac{P_{\max}}{1 + \exp(-k_p(x - x_{0,p}))} + p_0, \quad (1)$$

$$l(x) = \frac{L_{\max}}{1 + \exp(-k_l(x - x_{0,l}))} + l_0, \quad (2)$$

$$r(x) = \frac{R_{\max}}{1 + \exp(-k_r(x - x_{0,r}))} + r_0, \quad (3)$$

where P_{\max} , L_{\max} , and R_{\max} denote the saturation magnitudes of power consumption, latency, and throughput, respectively; k_p , k_l , and k_r control the sharpness of the transitions; $x_{0,p}$, $x_{0,l}$, and $x_{0,r}$ represent the characteristic batch size thresholds at which these transitions occur; and p_0 , l_0 , and r_0 are offset terms.

The fitted relationships for the three Llama models are shown in Fig. 3, while the fitting results for the two Qwen models, which exhibit similar trends, are provided in Fig. 10 in Appendix A. The measurement data (shown as solid dots) are obtained by averaging the raw GPU measurements over the entire observation horizon of each experiment in the ML.ENERGY benchmark dataset.

As batch size increases, GPU power consumption rises monotonically and eventually saturates. Inter-token latency also increases with batch size, with a nonlinear growth as the

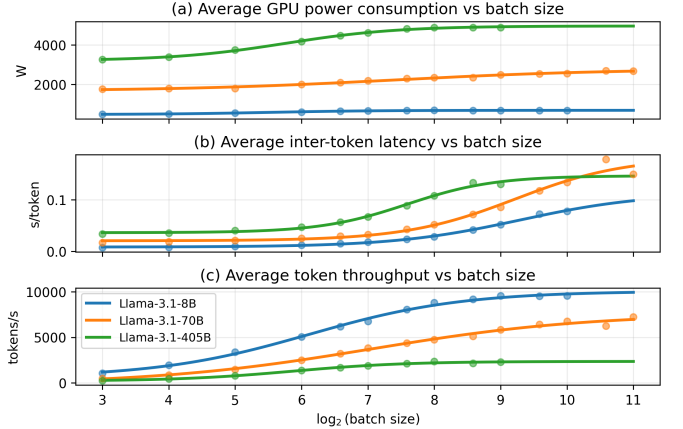


Fig. 3. Fitted relationships between batch size and performance metrics for three models in the Llama 3.1 family [17].

system approaches saturation. In contrast, token throughput initially increases rapidly with batch size, but exhibits diminishing marginal gains at larger batch sizes. These trends are consistent across model scales, although larger models operate at higher power and latency levels and reach saturation at smaller batch sizes. Overall, Fig. 3 demonstrates batch size is an effective control knob that induces predictable trade-offs among power, latency, and throughput with nonlinear impact.

III. GRID- AND USER-AWARE BATCH SIZE OPTIMIZATION

A. Batch Size Optimization Model

This section formulates GPU batch size control as an optimization problem, beginning with the power system model with data center load. Consider a data center connected to a single node in a three-phase distribution network with M buses. Let $\mathbf{v}_t \triangleq [\mathbf{v}_t^A, \mathbf{v}_t^B, \mathbf{v}_t^C]^\top \in \mathbb{R}^{3M}$ denote the stacked three-phase voltage magnitudes, where $\mathbf{v}_t^\phi \in \mathbb{R}^M$ collects voltages on phase $\phi \in \{A, B, C\}$. The phase-wise active and reactive power consumptions are $\mathbf{p}_t \triangleq [p_t^A, p_t^B, p_t^C]^\top$ and $\mathbf{q}_t \triangleq [q_t^A, q_t^B, q_t^C]^\top$, and a constant power factor PF is assumed for all phases, such that $q_t^\phi = \tan(\arccos(\text{PF})) p_t^\phi$. The mapping from \mathbf{p}_t and \mathbf{q}_t to \mathbf{v}_t is well established in power system modeling and simulation frameworks [22].

Assume the data center runs inference workloads for N distinct LLM models. Model i is deployed using w_i identical replicas, each assigned the same number of GPUs, and the vector $\mathbf{w} \triangleq [w_1, \dots, w_N]^\top$ denotes the replica counts. Under replica-based scaling, the time-averaged total power consumption and aggregate token throughput of model i scale approximately linearly with w_i , while instantaneous power may deviate from linear scaling due to temporal misalignment of short-term fluctuations across replicas. Because replicas operate in parallel, the ITL of each model does not scale with w_i . Accordingly, we use p_i , r_i , and l_i to denote the aggregate power consumption, total token throughput, and average ITL of model i , respectively.

For simplicity, we assume that all GPUs assigned to the same model are assumed to share a common batch size configuration. Let $\mathbf{b} \triangleq [b_1, \dots, b_N]^\top$ denote the batch size vector, where each b_i takes discrete values and is restricted

to powers of two, with batch size updates applied almost immediately after the control signals are sent to GPUs. To enable continuous optimization, we introduce the relaxed decision variable $\mathbf{x} \triangleq [x_1, \dots, x_N]^\top$, where x_i approximates $\log_2(b_i)$. Since key GPU performance metrics scale smoothly in the log batch size domain, formulating the control problem in terms of \mathbf{x} yields well-conditioned control actions.

The optimal batch size configuration can be determined by solving the following problem over \mathbf{x} at each control interval:

$$\max_{\mathbf{x}} \sum_{i=1}^N r_i(x_i) - \gamma \|\mathbf{x} - \mathbf{x}_t\|_2^2 \quad (4a)$$

$$\text{s.t. } \underline{\mathbf{v}} \leq \mathbf{v}(\mathbf{p}(\mathbf{x}), \mathbf{q}) \leq \bar{\mathbf{v}} \quad (\underline{\boldsymbol{\lambda}}, \bar{\boldsymbol{\lambda}}) \quad (4b)$$

$$l_i(x_i) \leq L_{\text{th},i}, \quad \forall i \quad (\mu_i) \quad (4c)$$

$$\underline{x}_i \leq x_i \leq \bar{x}_i, \quad \forall i, \quad (4d)$$

where $\underline{x}_i = \log_2(b_i)$ and $\bar{x}_i = \log_2(\bar{b}_i)$ denote the lower and upper bounds on the relaxed batch size variable for model i .² The optimization model's objective in (4a) aims to maximize the aggregate token throughput across all LLM models, which aligns with a fundamental operational goal of modern data centers. The regularization term $\gamma \|\mathbf{x} - \mathbf{x}_t\|_2^2$, with $\gamma > 0$, penalizes large deviations of the current decision variable \mathbf{x} from the previous control action \mathbf{x}_t . This term discourages abrupt changes in batch size decisions across successive control intervals, thereby promoting smoother and more stable GPU operation and corresponding power trajectories.

Moreover, the optimization model explicitly captures the coupling among three stakeholders: the power grid, the data center operator, and LLM service users. From the grid perspective, the voltage constraints in (4b) enforce three-phase voltage limits at all buses in the distribution system and are associated with dual variables $\underline{\boldsymbol{\lambda}}, \bar{\boldsymbol{\lambda}} \in \mathbb{R}_+^{3M}$. From the users' perspective, the latency constraints in (4c) impose per-model quality-of-service requirements, with dual variables $\mu_i \geq 0$. The mean inter-token latency threshold $L_{\text{th},i}$ may vary across models to reflect heterogeneity in LLM architectures and service-level objectives. From the data center operator's perspective, these constraints are jointly balanced against the throughput-maximization objective, enabling batch size decisions that simultaneously respect grid reliability and user experience.

B. Batch Size Control via Online Feedback Optimization

Since the batch size optimization in (4) is formulated as a continuous relaxation of an inherently integer-valued decision problem, discrepancies inevitably arise between the expected output and the realized behavior of the coupled user-GPU-grid system. Moreover, additional mismatches may be introduced by actuation delays, workload stochasticity, and unmodeled system dynamics. Online feedback optimization (OFO) inherently mitigates these issues by updating batch size decisions directly from real-time system measurements, rather than relying on exact model fidelity. This feedback-driven structure renders OFO robust to modeling inaccuracies and implementation imperfections.

²We use $b_i = 8$, as going lower doesn't reduce ITL while hurting throughput significantly. \bar{b}_i is set as the largest batch size that fits in GPU memory.

We adapt the classic OFO implementation in [23] to solve (4) and add a step for discrete actuation after that. At each control interval $t = 0, 1, 2, \dots$, the OFO controller executes the following steps.

Step 1: Measurement: The controller measures the three-phase voltage magnitudes at all buses, denoted by $\hat{\mathbf{v}}_t$, and the mean ITL of each LLM model, denoted by $\hat{l}_{i,t}$.

Step 2: Dual Variable Updates: The dual variables associated with the voltage and latency constraints are updated via projected gradient ascent:

$$\underline{\boldsymbol{\lambda}}_{t+1} = [\underline{\boldsymbol{\lambda}}_t + \rho_v (\underline{\mathbf{v}} - \hat{\mathbf{v}}_t)]_+, \quad (5)$$

$$\bar{\boldsymbol{\lambda}}_{t+1} = [\bar{\boldsymbol{\lambda}}_t + \rho_v (\hat{\mathbf{v}}_t - \bar{\mathbf{v}})]_+, \quad (6)$$

$$\mu_{i,t+1} = [\mu_{i,t} + \rho_l (\hat{l}_{i,t} - L_{\text{th},i})]_+, \quad \forall i, \quad (7)$$

where $\rho_v > 0$ and $\rho_l > 0$ are dual step sizes, and $[\cdot]_+$ denotes element-wise projection onto the nonnegative orthant.

Step 3: Primal Update in Log₂ Batch Size Space: The relaxed primal decision variable \mathbf{x} is updated via projected gradient descent:

$$\mathbf{x}_{t+1} = \Pi_{[\underline{\mathbf{x}}, \bar{\mathbf{x}}]} (\mathbf{x}_t - \rho_x \nabla_{\mathbf{x}} \mathcal{L}(\mathbf{x}_t, \underline{\boldsymbol{\lambda}}_{t+1}, \bar{\boldsymbol{\lambda}}_{t+1}, \mu_{t+1})), \quad (8)$$

where $\rho_x > 0$ is the primal step size, \mathcal{L} is the Lagrangian function associated with (4), and $\Pi_{[\underline{\mathbf{x}}, \bar{\mathbf{x}}]}(\cdot)$ denotes element-wise projection onto the box constraints $\underline{x}_i \leq x_i \leq \bar{x}_i$. The derivation of $\nabla_{\mathbf{x}} \mathcal{L}$ is provided in Section III-C.

Step 4: Discrete Actuation (Mapping \mathbf{x}_{t+1} to \mathbf{b}_{t+1}): The OFO update produces a continuous decision $\mathbf{x}_{t+1} \in \mathbb{R}^N$, whereas the GPU runtime requires discrete batch size settings. We therefore map each component to the nearest integer in log₂ scale and convert back to batch size:

$$\tilde{x}_{i,t+1} = \text{round}(x_{i,t+1}), \quad b_{i,t+1} = 2^{\tilde{x}_{i,t+1}}, \quad \forall i. \quad (9)$$

The resulting batch size vector $\mathbf{b}_{t+1} = [b_{1,t+1}, \dots, b_{N,t+1}]^\top$ is then applied to the GPU servers.

In summary, OFO enables the data center operator to iteratively adjust GPU batch sizes using real-time voltage and latency feedback, without requiring an exact or static system model. This makes OFO particularly well suited for real-time G2G coordination under practical implementation constraints.

C. Gradient Derivation with Respect to Batch Size

The proposed formulation in (4) is fully differentiable with respect to \mathbf{x} . Accordingly, the associated Lagrangian function can be written as

$$\begin{aligned} \mathcal{L}(\mathbf{x}, \underline{\boldsymbol{\lambda}}, \bar{\boldsymbol{\lambda}}, \mu) = & - \sum_{i=1}^N r_i(x_i) + \gamma \|\mathbf{x} - \mathbf{x}_t\|_2^2 \\ & + \bar{\boldsymbol{\lambda}}^\top [\mathbf{v}(\mathbf{p}(\mathbf{x}), \mathbf{q}) - \bar{\mathbf{v}}] + \underline{\boldsymbol{\lambda}}^\top [\underline{\mathbf{v}} - \mathbf{v}(\mathbf{p}(\mathbf{x}), \mathbf{q})] \\ & + \sum_{i=1}^N \mu_i (l_i(x_i) - L_{\text{th},i}). \end{aligned} \quad (10)$$

Let $\boldsymbol{\eta} \triangleq \bar{\boldsymbol{\lambda}} - \underline{\boldsymbol{\lambda}} \in \mathbb{R}^{3M}$. The partial derivative of the Lagrangian with respect to x_i is

$$\begin{aligned} \frac{\partial \mathcal{L}}{\partial x_i} = & - \frac{dr_i(x_i)}{dx_i} + 2\gamma(x_i - x_{t,i}) + \mu_i \frac{dl_i(x_i)}{dx_i} \\ & + \boldsymbol{\eta}^\top \frac{\partial \mathbf{v}}{\partial \mathbf{p}} \frac{\partial \mathbf{p}(\mathbf{x})}{\partial x_i}. \end{aligned} \quad (11)$$

Under a three-phase linearized distribution flow (LinDist-Flow) approximation [24], and assuming that power injections at all non-data-center buses remain constant, the bus voltage magnitudes changes from time t to $t + 1$ can be expressed as approximately affine functions of the power consumptions at the data center bus:

$$\mathbf{v}_{t+1} = \mathbf{v}_t - \mathbf{R} \Delta \mathbf{p}_t - \mathbf{X} \Delta \mathbf{q}_t, \quad (12)$$

where $\Delta \mathbf{p}_t = \mathbf{p}_{t+1} - \mathbf{p}_t$ and $\Delta \mathbf{q}_t = \mathbf{q}_{t+1} - \mathbf{q}_t$ denote the changes in active and reactive power consumptions at the data center bus. The sensitivity matrices $\mathbf{R}, \mathbf{X} \in \mathbb{R}^{3M \times 3}$ capture both within-phase and cross-phase voltage responses to variations in active and reactive data center load. Therefore, the voltage sensitivity with respect to active power becomes

$$\mathbf{H} \triangleq \frac{\partial \mathbf{v}}{\partial \mathbf{p}} = -\mathbf{R} - \tan(\arccos(\text{PF})) \mathbf{X} \in \mathbb{R}^{3M \times 3}. \quad (13)$$

Since model i may be executed on GPUs connected to different phases $\phi \in \{A, B, C\}$ of the power system, we introduce a phase-allocation weight vector $\mathbf{e}_i = [e_{i,A}, e_{i,B}, e_{i,C}]^\top \in \mathbb{R}^3$ where $e_{i,\phi}$ denotes the fraction of GPUs assigned to model i that are connected to phase ϕ . Therefore, we have

$$\frac{\partial \mathbf{p}(\mathbf{x})}{\partial x_i} = \mathbf{e}_i \frac{dp_i(x_i)}{dx_i}, \quad (14)$$

Given the logistic functions in (1), (2), and (3) which are the functions of power, latency, and throughput for one replica of model deployment, we obtain the gradient for the power, latency, and throughput of all replicas

$$\frac{dp_i(x_i)}{dx_i} = P_{\max} k_p w_i \frac{\exp(-k_p(x_i - x_{0,p}))}{(1 + \exp(-k_p(x_i - x_{0,p})))^2}, \quad (15)$$

$$\frac{dl_i(x_i)}{dx_i} = L_{\max} k_l \frac{\exp(-k_l(x_i - x_{0,l}))}{(1 + \exp(-k_l(x_i - x_{0,l})))^2}, \quad (16)$$

$$\frac{dr_i(x_i)}{dx_i} = R_{\max} k_r w_i \frac{\exp(-k_r(x_i - x_{0,r}))}{(1 + \exp(-k_r(x_i - x_{0,r})))^2}. \quad (17)$$

In summary, we obtain the gradient of Lagrangian with respect to x_i as

$$\begin{aligned} \frac{\partial \mathcal{L}}{\partial x_i} = & 2\gamma(x_i - x_{t,i}) \\ & - R_{\max} k_r w_i \frac{\exp(-k_r(x_i - x_{0,r}))}{(1 + \exp(-k_r(x_i - x_{0,r})))^2} \\ & + \boldsymbol{\eta}^\top \mathbf{H} \mathbf{e}_i P_{\max} k_p w_i \frac{\exp(-k_p(x_i - x_{0,p}))}{(1 + \exp(-k_p(x_i - x_{0,p})))^2} \\ & + \mu_i L_{\max} k_l \frac{\exp(-k_l(x_i - x_{0,l}))}{(1 + \exp(-k_l(x_i - x_{0,l})))^2}. \end{aligned} \quad (18)$$

This gradient captures the trade-offs among throughput maximization, latency constraints, voltage regulation, and penalties on large batch-size adjustments.

TABLE II
LLM INFERENCE WORKLOADS AND MODEL-SPECIFIC PARAMETERS IN NUMERICAL EXPERIMENTS

Model name	Replica Count	GPUs per replica	L_{th} (s)
Llama 3.1 8B	720	1	0.08
Llama 3.1 70B	180	4	0.10
Llama 3.1 405B	90	8	0.12
Qwen3-30B A3B	480	2	0.06
Qwen3 235B A22B	210	8	0.14

IV. NUMERICAL EXPERIMENTS

A. Data Center Power Profile Generation

A key challenge in numerical studies of data centers is the lack of publicly available, high-resolution power measurements that capture responses to inference-level control knobs such as batch size. Existing datasets (e.g., the MIT Supercloud Dataset [25]) characterize aggregate behavior but do not resolve control-induced power dynamics. To address this gap, we develop a cluster simulator based on real measurement data from [10], [13] to emulate realistic GPU responses (including power, ITL, and throughput) to batch-size control.

Synthetic load generation is guided by realism and diversity. Realism is modeled by superimposing multiple replica-level GPU power traces with randomly shifted start times, rather than simply scaling up a single trace, thereby capturing asynchronous arrivals and avoiding unrealistically amplified transients. Moreover, time-varying ITL is explicitly modeled. Historical ITL measurements exhibit heavy-tailed behavior, which we capture using a weighted mixture of two lognormal distributions per batch size, as shown in Fig. 4. Replica-level ITLs are sampled and averaged at each control interval to obtain model-level ITL for latency evaluation. Diversity is introduced through both fast and slow power variations. Fast transients arise from a temporary training workload running at the same time as inference, representing events such as training interruptions or resumptions, while slower variations are generated by gradually reducing the number of active LLM inference replicas to mimic time-varying request arrival rates.

The simulated data center has an aggregate capacity of approximately 5 MW and consists of 900 servers (8 GPUs each), evenly distributed across three phases. A constant base load of 0.5 MW per phase is included to represent ancillary infrastructure such as cooling, accounting for roughly 30% of total consumption [26]. We consider five heterogeneous LLM inference workloads (detailed in Table II), running together over a 60-minute horizon with 0.1 s resolution. Each model is assigned an initial replica count and a latency threshold L_{th} , with larger models serving fewer users and tolerating higher latency. The resulting configuration occupies 600 servers, providing sufficient GPU flexibility for voltage regulation. A transient training workload is added over $t = 1000$ to 2000 s using the rest 300 servers, and inference demand is linearly reduced from $t = 2500$ to 3000 s, producing both short-term variability and sustained power shifts that induce significant voltage dynamics in the distribution system.

We use this workload pattern for subsequent evaluations. Fig. 5(a) shows the resulting power profile and average ITL

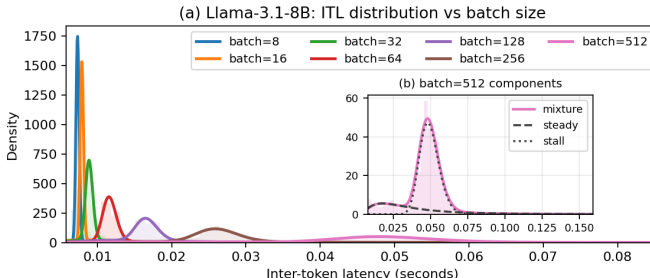


Fig. 4. Fitted ITL distributions across batch sizes for the Llama 3.1 8B model.

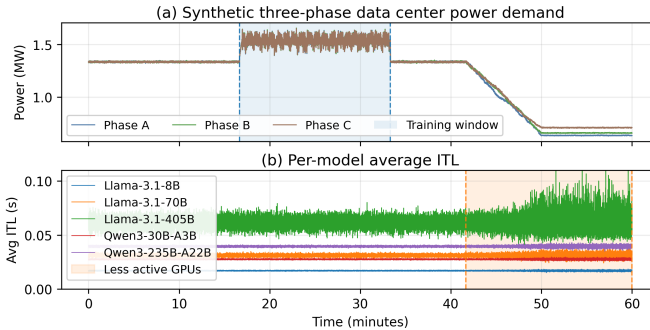


Fig. 5. Synthetic data center power and average ITL with a fixed batch size of 128 for all LLM models.

for a benchmark case with fixed batch size 128. Also, as shown by Fig. 5(b), the variability of per-model average ITL increases as the number of active GPUs decreases (orange area) due to reduced statistical averaging across servers.

B. Power System Simulation via OpenDSS

We evaluate voltage impacts using the IEEE 13-bus distribution feeder [27], with the data center connected at Bus 671 and operating at a constant power factor of $\text{PF} = 0.95$. The topology of the IEEE 13-bus feeder with a data center load is shown in Fig. 6. Bus 650 serves as the upstream substation and voltage reference, with its voltage regulated by the transmission system and thus weakly influenced by downstream load variations. Voltage regulation within the feeder is primarily provided by the step-voltage regulator between Bus 650 and Bus 632, whose tap operations produce discrete voltage changes at the regulator bus in response to sustained load variations. Thus, the voltage at the regulator bus reflects discrete changes corresponding to tap operations. Distribution system simulations are performed via the OpenDSSDirect.py interface [28].

As a baseline with no GPU flexibility, we simulate the system using the synthetic data center power profiles in Fig. 5(a), where voltage regulation is provided solely by tap changes of step-voltage regulator. Consistent with standard operating practice, tap changes are subject to a minimum dwell time of 30 minutes to limit mechanical wear, and we assume the earliest tap operation is permitted at $t = 25$ min. Figure 7 shows the resulting voltage trajectories on phases A–C at selected buses. Although tap actions correct sustained voltage deviations at $t = 25$ min and $t = 55$ min, the enforced delay leads to temporary voltage violations following data center

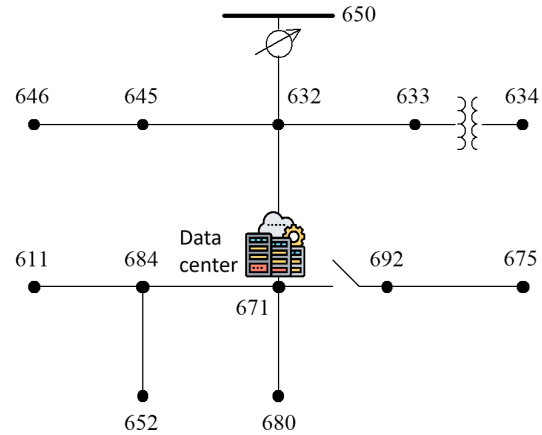


Fig. 6. IEEE 13-bus distribution feeder with data center load at Bus 671.

load changes, motivating the use of GPU flexibility as a fast complementary voltage regulation resource.

C. Batch Size Optimization Results

Voltage regulation with GPU flexibility is implemented using an OFO controller with primal step size $\rho_x = 0.1$, dual step sizes $\rho_v = \rho_l = 1$, and objective weight $\gamma = 0.1$, operating at a 1 s control interval. For all models, batch sizes are selected from the discrete set $\{8, 16, 32, 64, 128, 256, 512\}$. The resulting voltage trajectories are shown in Fig. 8, and the corresponding GPU performance metrics are shown in Fig. 9.

To interpret the batch size trajectories in Fig. 9, we categorize controller actions into three regimes: throughput-driven, voltage-driven, and latency-driven, reflecting how the OFO controller balances data center performance objectives against grid and users' requirements.

Throughput-driven regions: When no constraints in (4) are active, or when constraint violations do not dominate the gradient $\nabla_x \mathcal{L}$ in (8), the OFO controller maximizes aggregate token throughput across all models. As shown in Fig. 9(a), throughput-driven regions appear before and after the training window, ensuring performance maximization during non-critical intervals. In our implementation, per-replica throughput is normalized to a maximum of one to enable fair aggregation across models; in practice, operators may apply model-specific throughput weights to reflect service priorities.

Voltage-driven regions: Voltage-driven actions occur during the abrupt undervoltage event near $t \approx 1000$ s and the gradual overvoltage event near $t \approx 3000$ s. The corresponding stepwise changes in per-replica power, highlighted in Fig. 9(b), reflect aggressive batch size reductions and increases, respectively. Comparing Fig. 7 and Fig. 8, GPU batch size control enables faster and smoother voltage recovery than tap changers, which are constrained by slow mechanical actuation. Notably, the overvoltage case illustrates that increasing GPU power consumption can also provide valuable grid support, a result of interest to both power system and computer engineering communities.

Latency-driven regions: As shown in Fig. 9(c), ITL variability increases significantly after $t \approx 3000$ s. This is because

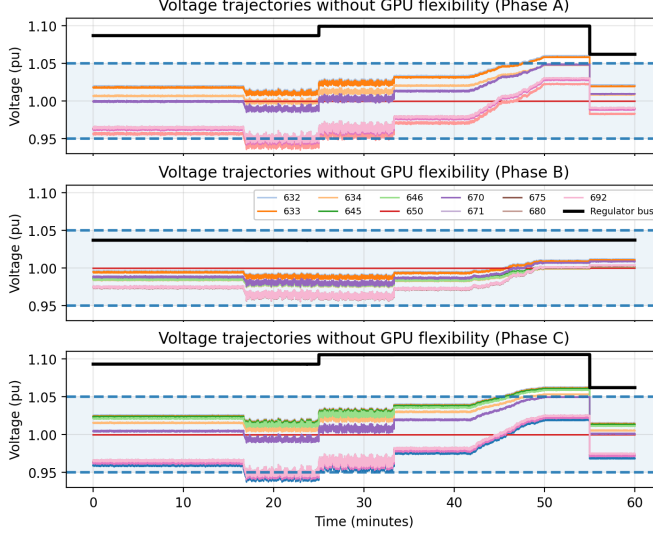


Fig. 7. Voltage trajectories in IEEE 13-bus system without GPU flexibility. The dashed lines indicate the voltage limits (0.95 and 1.05 pu).

TABLE III
VOLTAGE REGULATION PERFORMANCE COMPARISON

Case	Violation Time (s)	Worst V_{\min} (pu)	Worst V_{\max} (pu)	Integral Viol. (pu s)
No control, no tap	993.7	0.9350	1.0497	31.57
Tap change only	1095.5	0.9350	1.0632	43.74
GPU control only	78.0	0.9451	1.0508	0.0570

Note: Violation time is total voltage violation duration. Worst V_{\min}/V_{\max} are extrema across all buses and phases. Integral viol. is the time integral of out-of-limit voltage deviations.

empirically, larger batch sizes are associated with broader ITL distributions, resulting in greater latency fluctuations and a higher risk of violating latency constraints. Consequently, the batch size decisions in the green shaded region in Fig. 9 are primarily driven by latency regulation.

Finally, Table III quantitatively compares the voltage regulation performance of different cases. While tap-only control degrades voltage performance relative to the uncontrolled baseline due to actuation delays and overcorrection, GPU-based control reduces the integral voltage violation (capturing both the duration and magnitude of voltage deviations) by orders of magnitude without any tap operations during the simulation. This improvement arises from closed-loop feedback, which enables rapid correction of voltage deviations and avoids the prediction errors inherent in slow, open-loop voltage regulation devices. These results suggest that the inherent flexibility of GPUs can allow data centers to meet power system requirements without deploying additional flexible resources such as batteries.

V. CONCLUSION

This paper demonstrates the potential of GPU batch size control for distribution-level voltage regulation using real GPU measurement data from LLM inference workloads, showing that batch size is an effective and fast-acting control knob for grid support. Building on this insight, we propose an

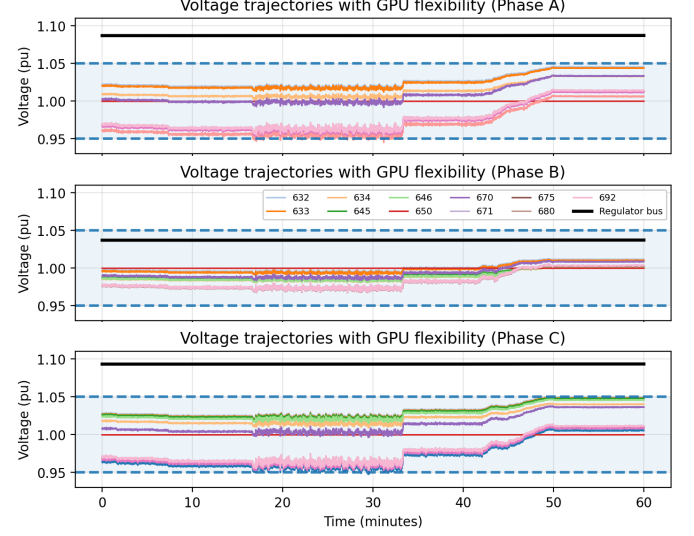


Fig. 8. Voltage trajectories in IEEE 13-bus system with GPU flexibility and no tap change. Voltages stay mostly within their limits.

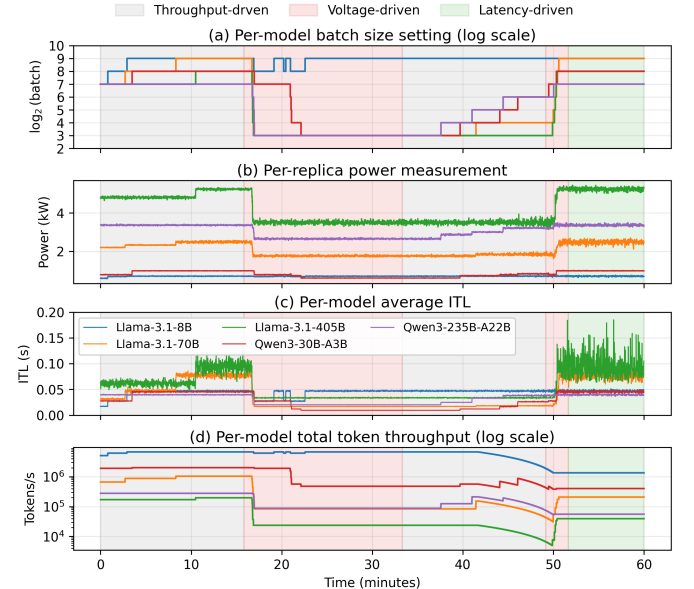


Fig. 9. OFO modulates batch size for each model to maximize throughput while meeting target inter-token latency constraints.

OFO framework that balances the requirements of the power grid, LLM service users, and data center operators by jointly considering voltage constraints, latency limits, and throughput objectives, while relying only on readily available grid measurements and avoiding the need for detailed grid information. A limitation of this study is that data center power, latency, and throughput dynamics are generated from pre-measured traces and fitted performance models, which may not capture all sources of variability present in real GPU operation. Future work includes extending to a hardware-in-the-loop setting, where GPU performance metrics are measured in real time and fully integrated into the control loop, enabling end-to-end validation under realistic operating conditions.

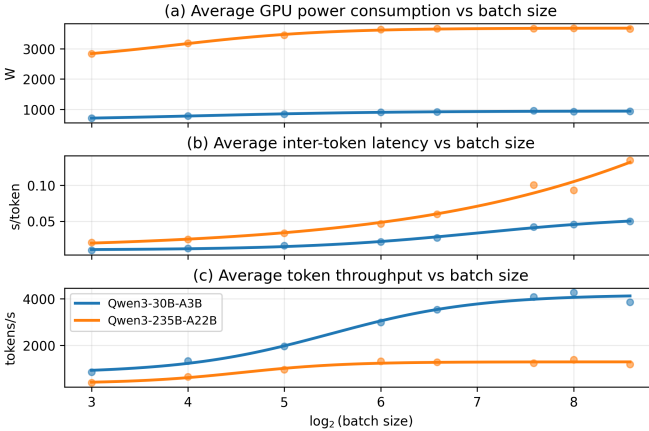


Fig. 10. Fitted relationships between batch size and performance metrics for two Qwen models.

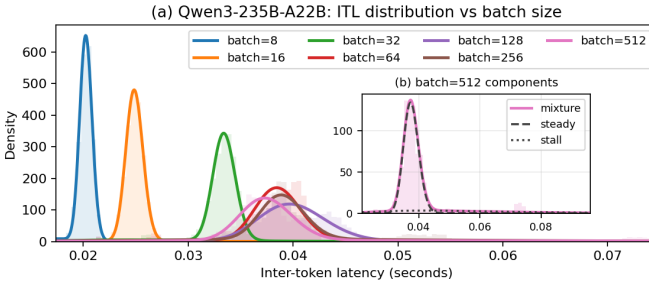


Fig. 11. Fitted ITL distributions across batch sizes for the Qwen3 235B A22B model.

APPENDIX

A. Additional GPU Measurement Data Plots

We present additional GPU measurement results for Qwen models to demonstrate that the key findings in the main text derived from Llama models generalize to other architectures. The fitted relationships between batch size and performance metrics for two Qwen models are shown in Fig. 10, which follow the same logistic functional form as (1)-(3).

In addition, Fig. 11 shows the fitted ITL distributions across batch sizes for the Qwen3 235B A22B model. As in Fig. 4, each distribution is modeled as a weighted mixture of two lognormal distributions. One stall distribution represents short-duration decoding events concentrated around the mean latency, while the steady distribution captures longer-lasting components that dominate the tail of the distribution. However, for batch sizes larger than 64, the distributions exhibit greater overlap in this case, which means that the ITL is not as sensitive to batch size increase as the Llama 3.1B 8B model.

REFERENCES

- [1] Masanet, Eric and Shehabi, Arman and Lei, Ning and Smith, Sarah and Koomey, Jonathan, “United states data center energy usage report,” Technical Report LBNL-2024-DataCenterReport, Lawrence Berkeley National Laboratory, 2024.
- [2] NVIDIA Corporation, “Nvidia h100 tensor core gpu.” <https://www.nvidia.com/en-us/data-center/h100/>, 2024.
- [3] X. Chen, X. Wang, A. Colacelli, M. Lee, and L. Xie, “Electricity demand and grid impacts of ai data centers: Challenges and prospects,” *arXiv preprint arXiv:2509.07218*, 2025.
- [4] C. Guille and G. Gross, “A conceptual framework for the vehicle-to-grid (v2g) implementation,” *Energy policy*, vol. 37, no. 11, pp. 4379–4390, 2009.
- [5] V. Dvorkin, “Agent coordination via contextual regression (agentconcur) for data center flexibility,” *IEEE Transactions on Power Systems*, 2024.
- [6] Y. Fu, X. Han, K. Baker, and W. Zuo, “Assessments of data centers for provision of frequency regulation,” *Applied Energy*, vol. 277, p. 115621, 2020.
- [7] Y. Xie, W. Cui, and A. Wierman, “Enhancing data center low-voltage ride-through,” *arXiv preprint arXiv:2510.03867*, 2025.
- [8] J. You, J.-W. Chung, and M. Chowdhury, “Zeus: Understanding and optimizing gpu energy consumption of dnn training,” in *20th USENIX Symposium on Networked Systems Design and Implementation (NSDI 23)*, pp. 119–139, 2023.
- [9] J.-W. Chung, Y. Gu, I. Jang, L. Meng, N. Bansal, and M. Chowdhury, “Reducing energy bloat in large model training,” *Proceedings of the 30th ACM Symposium on Operating Systems Principles*, 2024.
- [10] J.-W. Chung, J. J. Ma, R. Wu, J. Liu, O. J. Kweon, Y. Xia, Z. Wu, and M. Chowdhury, “The ML.ENERGY benchmark: Toward automated inference energy measurement and optimization,” in *NeurIPS Datasets and Benchmarks*, 2025.
- [11] Y. Chen and B. Zhang, “Voltage regulation in distribution systems with data center loads,” *arXiv preprint arXiv:2507.06416*, 2025.
- [12] P. Colangelo, A. K. Coskun, J. Megrue, C. Roberts, S. Sengupta, V. Sivaram, E. Tiao, A. Vijaykar, C. Williams, D. C. Wilson, *et al.*, “Ai data centres as grid-interactive assets,” *Nature Energy*, pp. 1–8, 2025.
- [13] “The ML.ENERGY benchmark.” <https://github.com/ml-energy/benchmark>.
- [14] R. C. Dugan and T. E. McDermott, “An open source platform for collaborating on smart grid research,” tech. rep., Electric Power Research Institute (EPRI), 2011.
- [15] W. Kwon, Z. Li, S. Zhuang, Y. Sheng, L. Zheng, C. H. Yu, J. Gonzalez, H. Zhang, and I. Stoica, “Efficient memory management for large language model serving with PagedAttention,” in *SOSP*, 2023.
- [16] A. Vaswani, N. Shazeer, N. Parmar, J. Uszkoreit, L. Jones, A. N. Gomez, L. Kaiser, and I. Polosukhin, “Attention is all you need,” in *NeurIPS*, 2017.
- [17] A. . M. Llama Team, “The llama 3 herd of models,” *arXiv preprint arXiv:2407.21783*, 2024.
- [18] N. Shazeer, A. Mirhoseini, K. Maziarz, A. Davis, Q. Le, G. Hinton, and J. Dean, “Outrageously large neural networks: The sparsely-gated mixture-of-experts layer,” *arXiv preprint arXiv:1701.06538*, 2017.
- [19] Q. Team, “Qwen3 technical report,” *arXiv preprint arXiv:2505.09388*, 2025.
- [20] J. Liu, J.-W. Chung, Z. Wu, F. Lai, M. Lee, and M. Chowdhury, “Andes: Defining and enhancing quality-of-experience in llm-based text streaming services,” *arXiv preprint arXiv:2404.16283*, 2024.
- [21] G.-I. Yu, J. S. Jeong, G.-W. Kim, S. Kim, and B.-G. Chun, “Orca: A distributed serving system for Transformer-Based generative models,” in *OSDI*, 2022.
- [22] J. J. Grainger and W. D. Stevenson, *Power System Analysis*. New York, NY, USA: McGraw-Hill, 1994.
- [23] L. Ortmann, A. Hauswirth, I. Caduff, F. Dörfler, and S. Bolognani, “Experimental validation of feedback optimization in power distribution grids,” *Electric Power Systems Research*, vol. 189, p. 106782, 2020.
- [24] L. Gan and S. H. Low, “Convex relaxations and linear approximation for optimal power flow in multiphase radial networks,” in *2014 power systems computation conference*, pp. 1–9, IEEE, 2014.
- [25] S. Samsi, M. L. Weiss, D. Bestor, B. Li, M. Jones, A. Reuther, D. Edelman, W. Arcand, C. Byun, J. Holodack, *et al.*, “The mit supercloud dataset,” in *2021 IEEE High Performance Extreme Computing Conference (HPEC)*, pp. 1–8, IEEE, 2021.
- [26] International Energy Agency, “Energy demand from ai and data centers,” *IEA Report*, 2025.
- [27] IEEE Distribution System Analysis Subcommittee, “Ieee 13 node test feeder,” tech. rep., IEEE Power & Energy Society, 2014.
- [28] M. J. O’Connell and contributors, “OpenDSSDirect.py: Direct python interface to opendss.” <https://github.com/dss-extensions/OpenDSSDirect.py>, 2020.